View metadata, citation and similar papers at core.ac.uk
brought to you by CORE
provided by Lancaster E-Prints

Welding dynamics in an atomistic model of an amorphous polymer blend with polymer-polymer interface

DMITRY G. LUCHINSKY[1,5], HALYNA HAFIYCHUK[1], VASYL HAFIYCHUK[1], KENTA CHAKI[2], HIROYA NITTA[2], TAKU OZAWA[2], KEVIN R. WHEELER[3], TRACIE J. PRATER[4], PETER V.E. MCCLINTOCK[5]

[1]KBR, Inc., ARC, Moffett Field, CA, USA,

[2]Materials Science Section, Engineering Technology Division, JSOL Corporation, JP

[3]NASA Ames Research Center, Moffett Field, CA, USA

[4]NASA Marshal Space Flight Center, Huntsville, AL, USA

[5]Department of Physics, Lancaster University, Lancaster, UK

Dated: May 12, 2020

ABSTRACT: We consider an atomistic model of thermal welding at the polymer-polymer interface of a polyetherimide/polycarbonate blend, motivated by applications to 3D manufacturing in space. We follow diffusion of semiflexible chains at the interface and analyze strengthening of the samples as a function of the welding time t_w by simulating the strain-stress and shear viscosity curves. The time scales for initial wetting, and for fast and slow diffusion, are revealed. It is shown that each component of the polymer blend has its own characteristic time of slow diffusion at the interface. Analysis of strain-stress demonstrates saturation of the Young's modulus at $t_w = 240$ ns, while the tensile strength continues to increase. The shear viscosity is found to have a very weak dependence on the welding time for $t_w > 60$ ns. It is shown that both strain-stress and shear viscosity curves agree with experimental data.

Keywords: polymer interfaces; polymer blend; molecular dynamics; reptation; welding; strength of the interface

INTRODUCTION

Understanding the properties of polymer-polymer interfaces represents a long-standing problem that is of both fundamental and technological importance[1–3]. For example, reptation, entanglement, and stress relaxation[1,4–8] determine the welding dynamics and parts strength in fused deposition modeling[9–11], which is of significant interest for space applications including NASA's In-Space Manufacturing (ISM) project that seeks to develop the materials and processes needed to provide an on-demand manufacturing capability for deep space exploration missions[12].

It is also known that the atomistic structure of polymers can substantially influence fundamental properties of welding dynamics mentioned above[13–15]. In particular, polyimides[15–17] and their blends[18–21] have recently attracted considerable attention due to the combination of processing, thermal, and mechanical properties suitable for aerospace applications. And the ISM project seeks to expand its on-orbit printing and recycling ecosystem by including blends of polyetherimide into the process. However, many issues related to optimization and predicting the quality of the parts remain unsolved[19–22] and their resolution could be facilitated by atomistic insight into the dynamics of polymer chains at an interface.

Molecular dynamics (MD) modeling could potentially provide the required atomic resolution[3,23–25] of the polymer interfaces and compliment technology development efforts. Most earlier research of this kind has been focused either on bulk polyimides[15–17,26–29] or on studies of the generic properties of polymer-polymer interfaces using coarse-grained models[3,23,24,30]. The latter simulations yield insight but do not, however, take into account limited flexibility and electrostatic properties of polymer chains that are of fundamental importance for chain diffusion[16,31–33]. An additional challenge is posed by the need to understand the structure-properties relationship at the interface of polymer blends. Although MD has been widely used to investigate bulk properties of blends[25,34–36] its application to modeling interfaces in blended polymer materials remains very limited. In particular, despite the fact that polyetherimide (PEI) polycarbonate (PC) mixtures are of significant importance in aerospace applications[37,38], there have been only a few MD studies of their bulk and interfacial properties. For example, Zhang and co-authors[27] published pioneering research on the

MD analysis of miscibility and on the anomalous effects observed in PEI/PC blends. The interfacial interactions between ULTEM and a variety of liquids have been evaluated[26] by use of molecular dynamics simulations. Further research into the dynamics of semiflexible chains at the interface of polymer blends in the presence of electrostatic interactions is much needed.

To address these issues we develop a fully atomistic model of the polymer-polymer interface in PEI/PC mixtures. The simulation of diffusing chains at the interface and relaxation of their distribution to the bulk state was limited to 240 ns. The welding analysis in this model has shown that initial wetting is followed by fast diffusion with Eyring's type jumps and then by slow diffusion of center-of-mass of polymer chains. The latter process was dominated by reptation with two characteristic timescales associated with two components of the blend. Existence of two slow timescales results in faster equilibration of the PC chains distribution, as compared to that of polyetherimide and in turn affects the dynamics of strengthening at welded interface.

The sample strength is characterized by simulation of uni-axial and shear deformations after quenching the samples to room temperature at $t_w = 60$ and 240 ns. It is shown that the Young's modulus of the quenched samples increases between $t_w = 60$ and $t_w = 240$ ns and saturates at $t_w = 240$ ns while, at the same time, the yield strength is continuing to increase. We further demonstrate that the dependence of the shear viscosity η on the shear rate in our model is linear on a log-log scale, corresponding to the expected shear-thinning behavior of the PEI/PC blends.

Both strain-stress curves and dependence of η on shear rate are shown to be in reasonable agreement with available experimental data. Thermal cycling was performed for an additional 1 μs to analyze the thermomechanical properties of welded samples, which were shown to be in agreement with experimental data, as will be discussed in detail elsewhere[39].

The model size was limited to 61912 atoms, which in turn imposes limitations on the cell size and on the timescale of the analysis. In this sense, the results presented should be considered complementary to those obtained for large coarse-grained models.

The paper is organized as follows. In the next section we describe the model of polymer-polymer interface. The "Results" section discusses the interfacial diffusion of polymer chains,

uni-axial sample deformation and the dependence of the shear viscosity on temperature and shear rate. Finally, the results are summarized and possible future work is outlined in the "Conclusions".

MODEL

According to Cicala et al.[38] the choices of high performance filaments for fused deposition modeling include Ultem 1000, Ultem 9085 and Polyphenylsulfone. Both Ultem grades are based on polyetherimide and they are certified for use in the automotive, medical and aerospace fields. Ultem 1000 is a pure PEI, while Ultem 9085 is a mixture of ∼80% PEI and ∼20% PC co-polymer blend incorporated for improved flow[20]. The present work focuses on the welding of materials such as Ultem 9085, studied through molecular dynamics simulations.

To model interface welding we prepared samples that consist of two amorphous cells with a mixture of polyetherimide and polycarbonate chains. Each cell had one flat face, see Fig. 1. Two cells were brought together to form an atomically flat interface, as shown in Fig. 1. We prepared two sets of polymer chains. The first set had 5 repeating monomer units for each PEI and PC chain. In the second set, the PEI and PC chains were 6 and 8 units long, respectively. Repeating units had 70 (PEI) and 35 (PC) atoms each, see corresponding atomic structure in Fig. S1 and results of calculations of partial charges in Tables 1 and 2 of the Supplementary Information (SI).

The resultant sample with the 1-st set of chains contained 41328 atoms, 96 PEI and 48 PC chains, and was of size $\sim 61 \times 61 \times 147$ Å^3 . The 3D image of the final sample is shown in Fig. S4 of the SI. Samples prepared with the 2-nd set of chains contained 61912 atoms, 130 PEI and 52 PC chains, and were of size $\sim 71 \times 71 \times 177$ Å^3.

The degree of polymerization (DP) at present is limited by the maximum size of the samples that could be processed in simulations. The resulting DP corresponds to the transition from oligomers to polymers. We note that the characteristic ratios for PC and PEI are 3-4 as estimated by Bicerano's group contribution method. The number of backbone bonds are 20 (PC) and 25 (PEI) for the models with the DP 5 meaning that the model polymers used

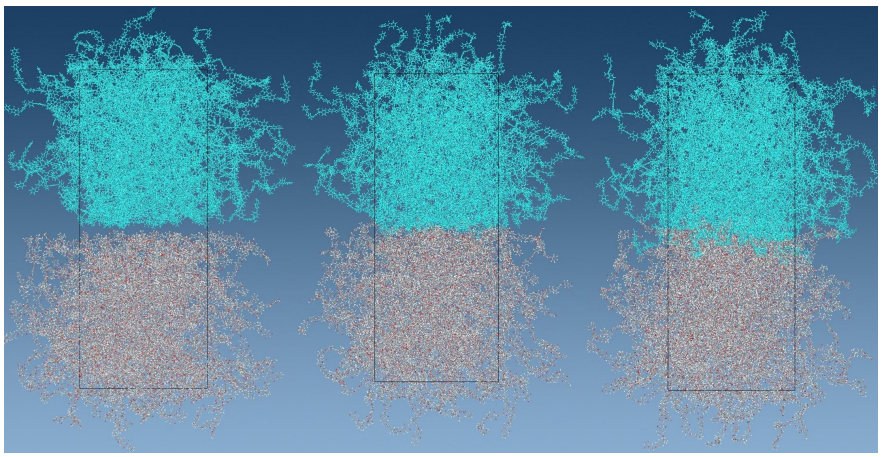

Figure 1: (left) Two atomistic amorphous cells of PEI/PC polymers blends (grey and cyan) combined in one chemical sample with atomically flat polymer-polymer interface. The samples are shown at $t_w = 0$ (left), at $t_w \approx 10$ ps (middle) and $t_w \approx 60$ ns (right). (color online)

in this study can behave like random polymer chains.

In the absence of experimental data demonstrating the dependence of the results on the DP we estimated this dependence using Fox-Flory theory[40]. According this theory both cases 5-5 and 6-8 (PEI-PC DP) are in the range ≥1000 g/mol where the dependence of the glass transition temperature T_g on the DP is approaching a plateau. In addition, the MD computation[27] of the solubility parameter χ of PEI and PC chains as a function of the DP indicates that the change from 5-5 to 6-8 (PEI-PC DP) in the model corresponds to the transition towards saturation of the χ. Comparison of the two models reveals similar quantitative features of the interface diffusion and allows us to assume that the captured features are robust.

Each cell was built using the software package J-OCTA[41] by placing at random polycarbonate and polyetherimide chains such that initial dilute mixture had 20 wt % PC and 80 wt % PEI and the initial sample density ≈ 0.65 g/cm^3. To prepare one nearly atomically flat surface (with normal vector parallel to the z-axis) in each cell we applied the Lennard-Jones (LJ) potential at this face while keeping the boundary conditions periodic in the X- and Y-directions and free in the Z-direction. The cells were relaxed compressed. and relaxed again using standard procedures[41] described in further details in section "Simulation details"

Table S3 of the SI.

The relaxation process was monitored by calculating potential energy, energy of non-bonding interaction, density, and radius of gyration of the PEI and PC chains as a function of time. These quantities level out by the end of the relaxation process. Note that in the actual manufacturing process the polymers at the interface are away from equilibrium (see more detailed discussion in the SI) and further analysis of the dependence of the interface diffusion on the distribution of the chains at the interface will be required in the future.

Finally, the interface welding was simulated by allowing polymer chains to diffuse freely at high temperature as shown in Fig. 1, see Table S4 of the SI. Top (cyan) and bottom (gray) cells in these sample were prepared as discussed above. We note that there is a second interface due to periodic boundary conditions in the merged system. However, initial entanglement at the second boundary is the same as in the bulk and initial stress relaxes fast to the bulk state. Welding takes place at the interface flat separated faces with initial gap shown in Fig. 1. and in what follows we focus on the analysis of this interface.

Simulation details

The welding simulations were conducted in an NPT ensemble with periodic boundary conditions using either LAMMPS[42,43] or GROMACS[44–46] or J-OCTA VSOP[41]. The LAMMPS simulations were performed on a supercomputer at the Ames Research Center[47] and High End Computing cluster at Lancaster University. GROMACS simulations were performed on Amazon Web Services that support GPU[48]. J-OCTA was used on a workstation. Further details are provided in the section "Simulation details" Tables S4 and S5 of the SI.

The limited size of the samples and periodic boundary conditions allow analysis of welding during a few hundred nanoseconds. In particular, simulations of welding in the 1st sample were performed at 600 K during 240 ns. After 60 ns and 240 ns, partially equilibrated samples were quenched to 300 K in 12 steps of 25K each. Additional thermal cycling of the smaller sample was performed between 300 K and 600 K with the time step varying between 12 ns and 25 ns. The initial temperature of the interface was chosen to correspond roughly to the actual welding process, in which an extrusion temperature is 623-653 K (i.e. well above $T_g = 459$ K) while the bed temperature is ~ 413 K (i.e. below T_g).

The temperature profile of the simulations is shown in Fig. S5 of the SI. The total time above the T_g during thermal cycling was ∼400 ns. Welded samples at different temperatures obtained during thermal cycling were used to estimate thermomechanical and spectral properties of the PEI/ PC blends as discussed in a separate paper[39].

The welding, quenching, and thermal cycling used an NPT ensemble i.e. keeping pressure, temperature, and the total number of particles fixed [1]. The quenched samples at time instances 60, 240 ns, and after thermal cycling with different thickness of the welded layer were used to study strain-stress and shear-viscosity - shear-rate relations of the blends.

The classical Hamiltonian of the polymer system used in this study is of the form[49]

$$\mathcal{H}(p,q) = K + U_{bond} + \sum\nolimits_{non-bond} \left[\frac{q_i q_j}{4\pi\varepsilon_0\varepsilon} + \frac{A_{ij}}{r_{ij}^{12}} - \frac{B_{ij}}{r_{ij}^{6}} \right] \tag{1}$$

where the first term K on the right-hand side is the kinetic energy of the system, the next term U_{bond} corresponds to bonding interactions between atoms in the polymer chain, and the last term corresponds to non-bonding interactions. Here r_{ij} is the distance between the i-th and j-th atoms, q_i is the atomic charge, ε_0 is the permittivity of free space, ε is the dielectric constant, and A_{ij} and B_{ij} are parameters of the LJ potential. In the simulations we use the Dreiding force field[50] and assign partial charges using the molecular orbital (MO) method with PM3 in MOPAC[51], see the SI for further details. Electrostatic interactions are calculated by the particle-mesh technique, particle-mesh Ewald (PME)[52] for GROMACS and particle-particle-particle-mesh Ewald[53] for VSOP and LAMMPS.

We note that Dreiding force field was used earlier[27,54] for molecular dynamic simulations of the polyetherimide. In[27] its performance was compared to that of the COMPASS[55] force field. It was found that Dreiding gave the most accurate estimation of solubility parameters of the present systems and provided much faster performance for simulation work on polymer blends. It was also successfully used in[25,56] to simulated epoxy thermosets with related structure of the polymer chains. However, this force field underestimates density by 10-15 %, see Fig. S6 of the SI, and to use Dreiding force field in this work we performed extensive validation of other thermo-mechanical properties of PEI/PC blends and found a reasonable agreement with available experimental data[57].

[1]Note that the interface temperature of the two filaments in the additive deposition process can be considered nearly fixed during the 300 ns used in MD simulations.

There are promising alternatives to Dreiding force field in terms of efficiency and accuracy[28,58,59]. The details of the validation and comparison with the performance of alternative force field will be reported elsewhere[39].

To estimate the strengthening of samples as a function of welding time we note that in the presence of deformation the internal energy of the system $E = \langle \mathcal{H} \rangle$ is related to the Gibbs G and Helmholtz F free energies as[60]

$$G = E - TS + \sigma_{ik} u_{ik} = F + \sigma_{ik} u_{ik}, \tag{2}$$

where S is the entropy, T is the temperature, and σ_{ik} and $u_{ik} = \frac{1}{2}\left(\frac{\partial u_i}{\partial x_k} + \frac{\partial u_k}{\partial x_i}\right)$ are respectively the stress and strain tensors given by[60]

$$\sigma_{ik} = \left(\frac{\partial F}{\partial u_{ik}}\right)_{T,N} \quad \text{and} \quad u_{ik} = \left(\frac{\partial G}{\partial \sigma_{ik}}\right)_{T,N}. \tag{3}$$

To account for the interface contribution to the overall stress we note also that the system consists of two bulk polymer samples and the interface. In general, the energy of such systems is a sum of three contributions[61]

$$E = E^L + E^s + E^R. \tag{4}$$

where the L, R, and s indices correspond respectively to the left, right, and surface components. In MD, the 6 components of the pressure tensor (negative of stress tensor) are calculated as[62]

$$P = \frac{1}{V} \sum_i \left(\frac{\langle p_i p_i \rangle}{m_i} + \sum_{k>i} \langle r_{ik} f_{ik} \rangle \right) \tag{5}$$

where $p_i = m_i v_i$ is the momentum of the i-th atom of mass m_i and velocity v_i, $r_{ik} = r_i - r_k$, and f_{ik} is the total force acting on the i-th atom.

Thus we see that the interface energy contributes to the value of the pressure tensor measured for the whole system. Changes of interfacial energy as a function of welding time can be detected by applying uni-axial or uni-diagonal deformation and measuring the corresponding pressure tensor. The gradient of the free energy at the sample interface is also a driving force for the diffusion that underlies the welding process. We will now discuss the welding dynamics observed in the simulations.

RESULTS

Diffusion at the interface

To resolve interfacial diffusion at the initial time we used the second, larger, sample with longer chains and with total number of atoms 61912. The interface was prepared and relaxed at a temperature 650 K, following the procedure described in the Model section. The interfacial dynamics in both samples was qualitatively similar.

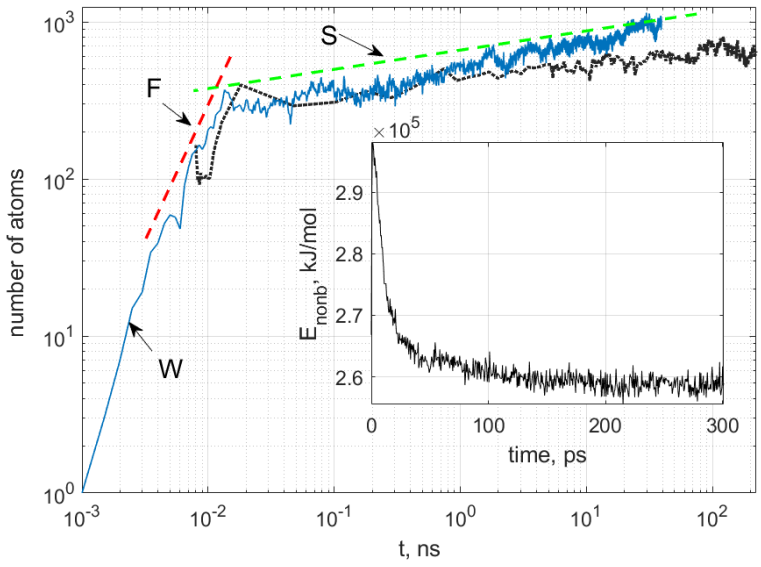

Figure 2: The number of atoms diffused across the interface from top to bottom (see Fig. 1) is shown by the solid line in comparison with the dynamics in the smaller sample (dotted line). Different regimes of diffusion are shown by labeled arrows: (W) wetting; (F) fast; and (S) slow diffusion. The "fast" and "slow" slopes are indicated by dashed lines. The inset shows the initial dynamics of the non-binding energy in the large sample corresponding to transition from "wetting' to "slow" diffusion regime.

As the samples are allowed to equilibrate, the first phenomenon observed is "wetting", when the two surfaces quickly come close to each other[1,63], on the time scale of a few picoseconds. The wetting process is governed by the electrostatic and van der Waals forces. The smaller the gap between two surfaces (assuming that Pauli repulsion for atoms in different

chains remains weak), the smaller is the total non-bonding energy of the sample, as shown in the inset of Fig. 2, see also video of "wetting" process in the SI.

Next, we observe a relatively fast diffusion of polymer chains on a time scale of ∼20-30 ps. The difference in the diffusion rates between "slow" and "fast" diffusion can be clearly seen in the figure as the difference between two slopes shown by dashed lines. We attribute the observed accelerated diffusion to the initial existence of un-equilibrated chain ends and "vacancies" on the both sides of the interface. As a result the diffusion is driven by both reptation and Eyring-type[64] jumps of the chain ends between quasi-equilibrium positions: see the SI for further illustration of this point.

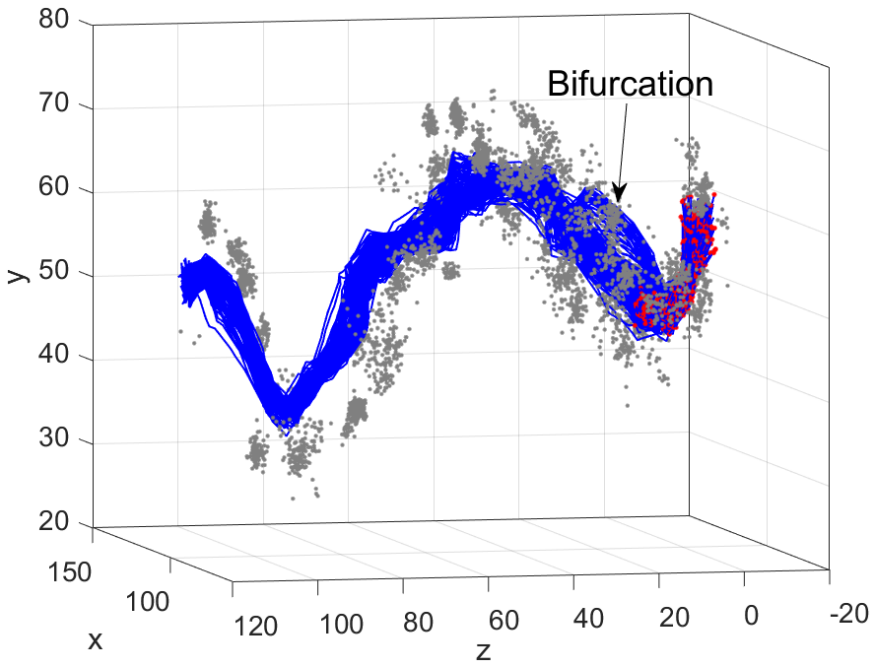

Figure 3: Reptation tube obtained by overlapping 138 snapshots of a single PEI chain. Gray dots show closet location of other chains that are entangled with selected PEI chain. Red dots show the location of the reduced units (see the SI for their definition) of the selected chain that crossed the interface. (color online)

Finally, a slow interfacial diffusion of the chains is found for $t_w > \sim 30$ ps, governed mainly by the reptation, cf.[33]. The transitions discussed are illustrated in Fig. 2 where the number of atoms crossing the interface from top to bottom (see Fig. 1) is shown as a function of time for both samples. Further details of the interfacial dynamics of atoms and chains are

shown in Fig. S7 of the SI.

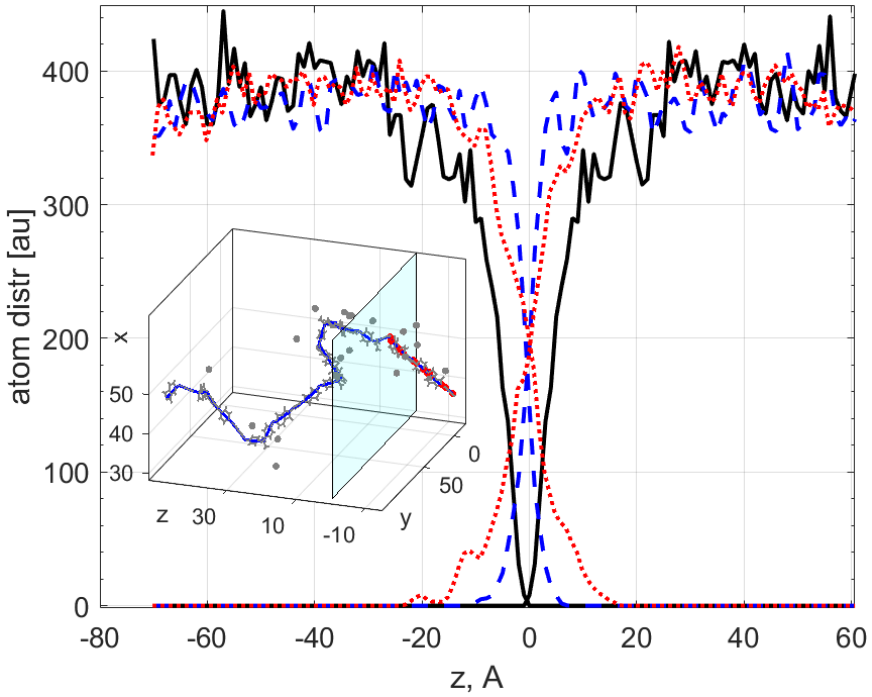

Figure 4: Atom density profiles of the polymers on both sides of the interface: (i) initial (black solid lines); (ii) at ∼125 ps (blue dashed lines); (iii) at ∼100 ns (red dotted lines). The inset depicts a single chain reptation at the interface from left to right through the transparent blue plane. The atomic structure of the chain is shown by thin gray lines indicating bonding between the atoms in the chain. The chain core (reduced chain) is shown by the blue solid line. The reduced sub-units of the chain that crossed the interface are shown by red dots. (color online)

The reptation tube of the PEI chain is shown in Fig. 3. It was obtained by overlaping 138 snapshots of the reduced chain shown in the inset of Fig. 4; see Fig. S8 and S9 of the SI online for a more detailed view. The clouds of gray dots show the closest location of the polymer chains entangled with this chain and restricting its motion. The distribution of the solid lines and the size of each cloud can also be used for estimations of the tube diameter as ∼10Å.

It can be seen from the figure that the reptation tube bifurcates between two locations near the interface. This bifurcation illustrates the Eyring-type[64] jumps of the chain ends

between quasi-equilibrium positions at the initial stage of the diffusion discussed here.

During reptation the semiflexible chain remains within a "tube" determined by the intersections with neighboring chains and the chain ends move slowly across the interface in random fashion. A snapshot of this motion is shown in the inset of Fig. 4 after ∼40 ns of welding. The thick lines in the inset show the reduced representation of the chain, see Fig. S8 and S9 of the SI. The gray dots show the locations of chains that constrain the motion of the selected chain. The cut-off distance in the search for chains entangled with the blue chain was ∼10 Å. The reduced units of the blue chain reptated through the interface are shown by red dots (color online). Note that, initially, the whole chain was on one side of the sample. Additional details of the tube properties and the relation between fully atomistic and reduced presentations of the chains are provided in Figs. S7, S8 and S9 of the SI, see also the 2-nd and 3-rd video links in the SI.

Profiles of the atomic densities on the two sides of the interface corresponding to the time scales discussed are shown in Fig. 4. It can be seen from the figure that the two samples are initially well separated, with zero density (ρ) at the interface and the gap at half bulk density ∼10Å. After ∼125 ps the interface density has nearly reached its bulk value. During the next ∼100 ns the interface density stays almost the same but the tails of the distributions extend to the other side by nearly 20 Å.

This extension of the distributions tails has a profound effect on the interface strength. Indeed, according to Wool[6] full strength is obtained when polymer filaments are inter-diffused to a distance equal to 81% of the radius of gyration (R_g). (Note, that for the semiflexible chains studied here Wool's criterion should be used only as a guiding approximation, see further discussion in the SI.) This condition means that the centers-of-mass distribution of the chains at the interface should approach its bulk value. In the large sample, the PEI chains extend from their center of mass by ∼60Å, while the PC chains extend approximately ∼30Å, see Fig. S10 and S11 of the SI.

The overlapping of cores of the distributions by ∼81 % of the R_g assumes that the maximum of the distribution for PEI chains approaches the interface by the distance $\sim 0.6R_g$. Therefore, we expect complete healing of the interface when the maximum (relative to the interface located at $z = 0$Å) chain extension in the z-direction is ∼40 Å. We observe, however,

a substantial slowing down of the tail extension beyond 20Å, which is attributable to the blend structure, with 80% of PEI and 20% of PC chains. The latter chains, being smaller and more flexible, diffuse faster towards the interface, while the stiffer and longer PEI chains need more time to equilibrate.

It is known that miscible[36] and immiscible[34] polymer blends possesses different local dynamics and a self concentration effect for the components. Here we reveal the effect of distinct segmental dynamics on welding and strengthening of polymer interfaces.

The two different timescales for inter-diffusion of PEI and PC chains were observed directly in simulations by following the center-of-mass (CM) distribution of individual chains in time, as shown in Fig. 5. It was found that the CM distribution of PC chains bridges the initial gap at the interface and becomes nearly uniform at a time of about 100 ns. The CM distribution of the PEI chains tends towards equilibrium, but remains nonuniform with a gap at the interface for up to 300 ns.

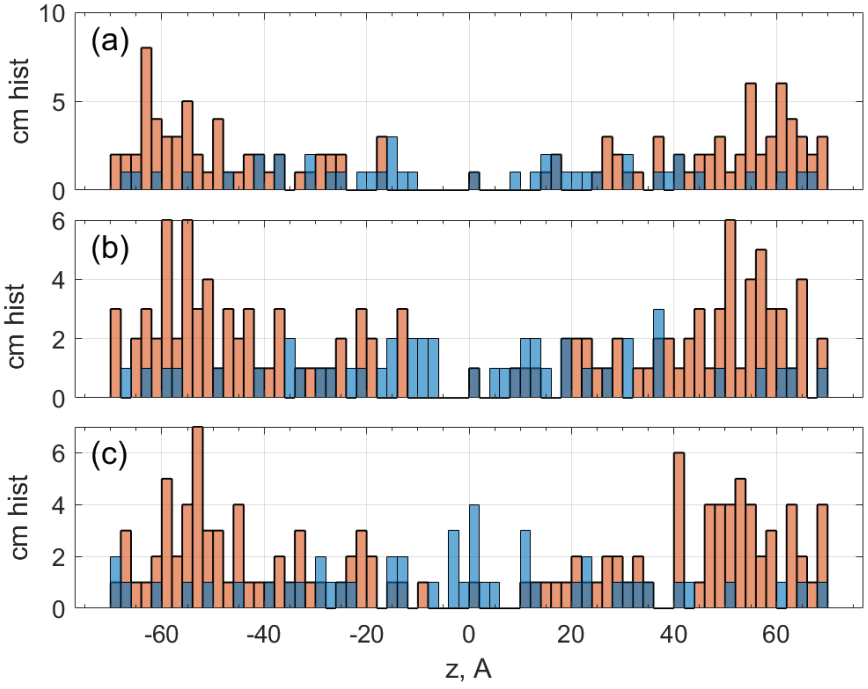

Figure 5: Histogram of the centers-of-mass of PEI (brown) and PC (blue) chains obtained in MD simulations for three different times: (a) initial state; (b) 300 ps; (c) 100 ns. (color online)

We conclude that the strength of the interface is approaching its bulk value as a function of time, but that the curing process remains incomplete. On the time scale of the simulations, the interface strength will be determined mainly by the inter-diffusion of PC chains and will be lower than that expected for polyetherimide. We now discuss the estimation of sample strength as a function of welding time, using MD simulations.

Strain-stress curve

The strain-stress curves of the samples were estimated by simulating uni-axial deformation at a constant rate in the Z-axis direction using a scenario developed by J-OCTA[41]. These simulations were performed in LAMMPS[65] using an NVT ensemble. The sample shape before and after the deformation is shown in Fig. S9 of the SI. The estimates are found to depend on the elongation rate v_e.

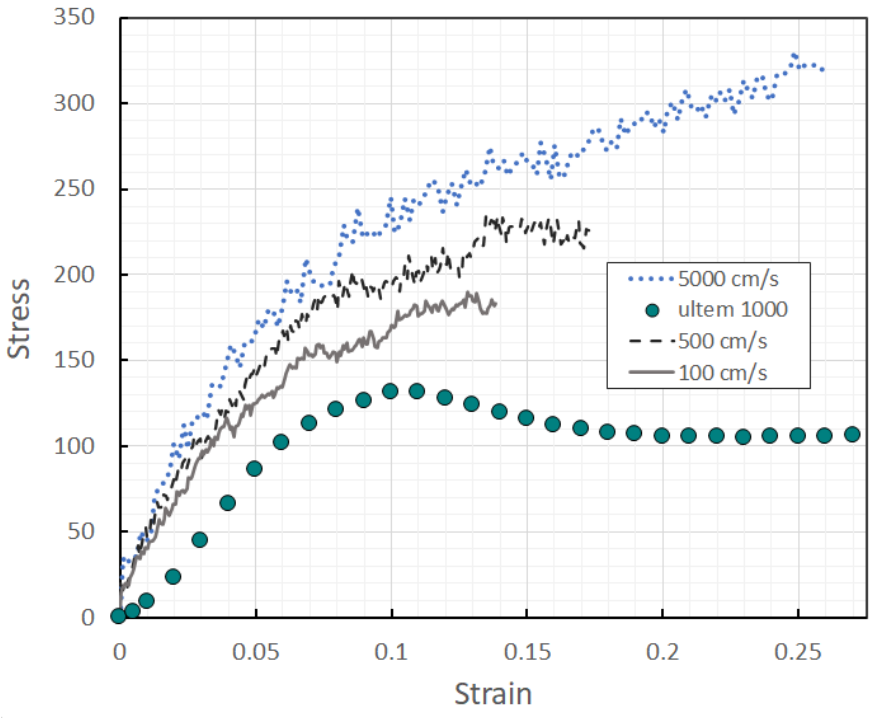

Figure 6: Dependence of the strain-stress curves on the elongation rate at $T = 300$ K (from top to bottom): 5000 cm/s; 500 cm/s; and 100 cm/s. The teal shaded circles show experimental results obtained[66] for Ultem 1000. (color online)

The strain-stress curves obtained in the MD simulations for three different elongation

rates are compared with experimental data in Fig. 6. The observed strong dependence of the strain-stress curves on elongation rate suggests that the higher Young's modulus obtained in MD simulations should be attributed to the large elongation rates and that agreement with the experimental results is semi-quantitative.

Dependence of the strain-stress curves on the welding time and the temperature is shown in Fig. 7. The left panel shows data obtained for an elongation rate of 5000 cm/s and $T = 300$ K while the right panel shows strain-stress curves obtained for an elongation rate of 100 cm/s and $T = 350$ K.

It can be seen from the figures that at $T = 300$ K both the Young's modulus and yield strength obtained in MD simulations are larger than those estimated from the experimental data for ULTEM 1000. It can also be seen that Young's modulus E is increased when the welding time is changed from 60 ns to 240 ns. The change of E is much less pronounced for further increase of welding time during thermal cycling. This observation is in agreement with the discussion of interfacial diffusion in the previous section.

When the sample temperature is increased to 350 K and the time step is reduced to 0.25 fs the values of Young's modulus and yield strength approach the experimentally estimated values. The change of Young's modulus as a function of welding time in this case is similar to that observed at 300 K indicating an increase of the interface strength of the sample as a function of the inter-diffusion time.

We note that the calculations were performed for a nominal Poisson's ratio of ULTEM 1000 $\nu = 0.36$[67], an assumption that becomes increasingly inaccurate because sample-breaking is initiated at the interface. For this reason the strain-stress curves obtained in MD are shown by dashed lines for large values of the strain.

The fact that the samples break at the interface indicates that it remains the weakest point of the whole structure, for all welding times used in the MD simulations. However, after additional thermal cycling no break up or breaking up at a different locations could be observed depending on the rate of elongation.

The value of Young's modulus $E \sim 3 - 4$ GPa estimated in MD simulations at 300 K is slightly larger than the value 2 – 2.5 GPa estimated based using open data[67].

The overall conclusion of this section is that fully atomistic MD simulations yield esti-

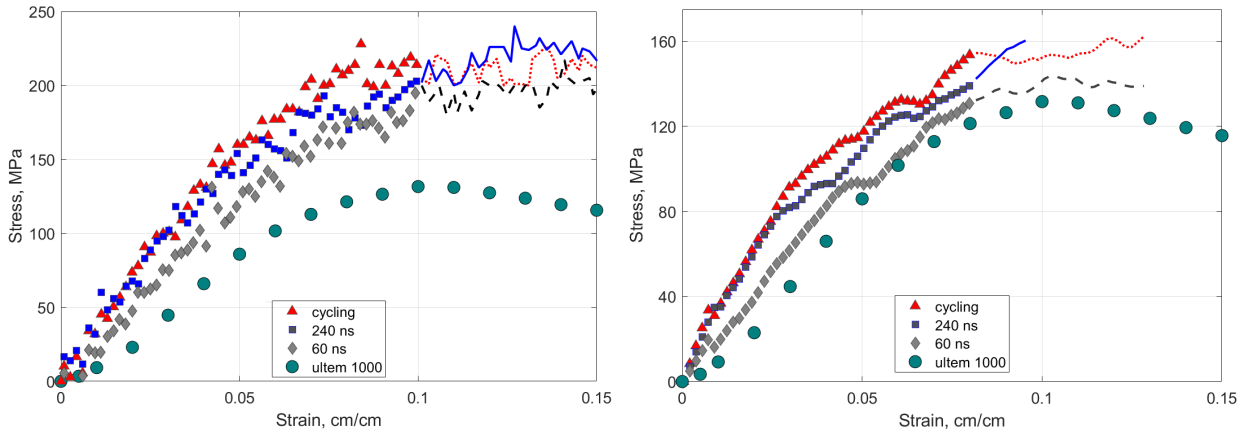

Figure 7: MD simulations of the strain-stress curves as a function of welding time: (i) 60 ns - grey diamonds; (ii) 240 ns - blue squares; (iii) after additional thermal cycling - purple triangles. (left) $v_e = 5000$ cm/s, $T = 300$ K. (right) $v_e = 100$ cm/s, $T = 350$ K.The experimental data[66] obtained for ULTEM 1000 are shown by teal-shaded circles. Dashed lines show extensions of the curves obtained in MD simulations beyond the point where the approximation of constant Poisson ratio breaks down.

mates of the Young's modulus and yield strength which are in semi-quantitative agreement with experimental data, and which reveal an increase of the interface strength as a function of welding time. We now consider the MD simulations of the shear viscosity in these samples.

Shear viscosity

Shear viscosity η is one of the most important properties of glassy polymer materials[68], in that it controls melt flow and is crucial for understanding the mechanism of the glass transition. To estimate shear viscosity we used NVE ensemble and applied shear deformation in GROMACS and LAMMPS. The shear deformation was applied in the XY plane along the Y direction parallel to the interface plane of the sample: see Fig. S10 of the SI. Simulations were performed for two samples quenched from 600 to 300 K, at welding times of $t_w = 60$ ns and 240 ns, using an algorithm proposed by J-OCTA[41]. The LAMMPS simulation yields the shear viscosity as a function of the shear rate γ and temperature, as shown in Fig. 8. The following features may be noted in the figure.

First, we observe that the dependence of η on the shear rate exhibits characteristic shear-

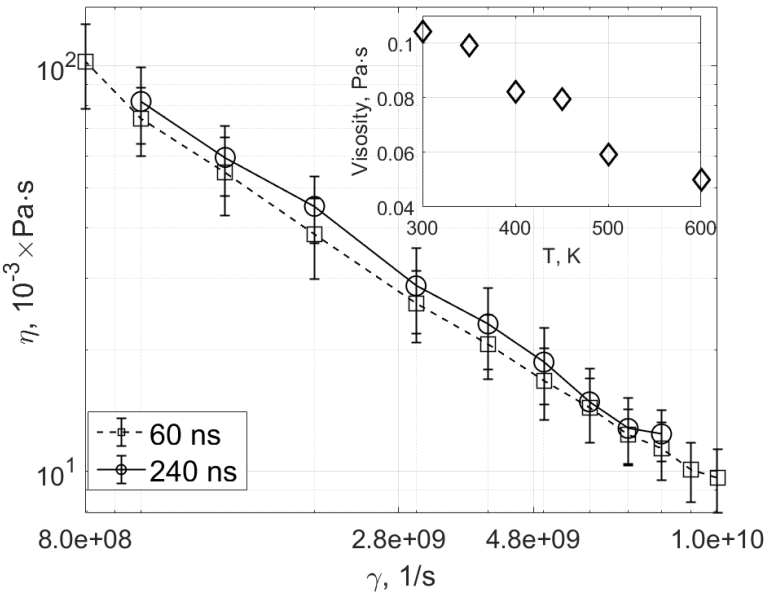

Figure 8: Shear viscosity η as a function of shear rate for smaller sample after 60 ns (open squares) and 240 ns (open circles) of healing. The inset shows shear viscosity as a function of temperature during quenching after 240 ns of welding for shear rate $\gamma \approx 8 \times 10^8$ 1/s.

thinning behavior[69] corresponding to a linear dependence of η on γ when plotted on a log-log scale. Secondly, we see that the shear viscosity calculated at 240 ns is slightly shifted towards larger values. However, the shift is small compared to the estimation error.

The latter result corroborate Eyring's view[64,70] of the interface viscosity (η_{int}) and our earlier discussions of the interface diffusion. He suggested that the interface viscosity is determined by the activation energy E_a of a molecule (or a chain end) to jump from one quasi-equilibrium position to a neighboring one. Initially the interface between two polymers is nearly atomically flat and the activation energy is small, resulting in smaller sample viscosity. Both E_a and η_{int} increase as functions of welding time. However, the η_{int} contribution to the overall viscosity of the sample is relatively small and it decreases with time due to the interface equilibration. As a result the observed shift of η is less than the measurement error.

The dependence of η on temperature is shown in the inset of Fig. 8 for shear rate $\gamma \approx 8 \times 10^8$ 1/s. It is evident that the temperature dependence of η is well resolved and that it exhibits the expected trend of decreasing as the temperature rises.

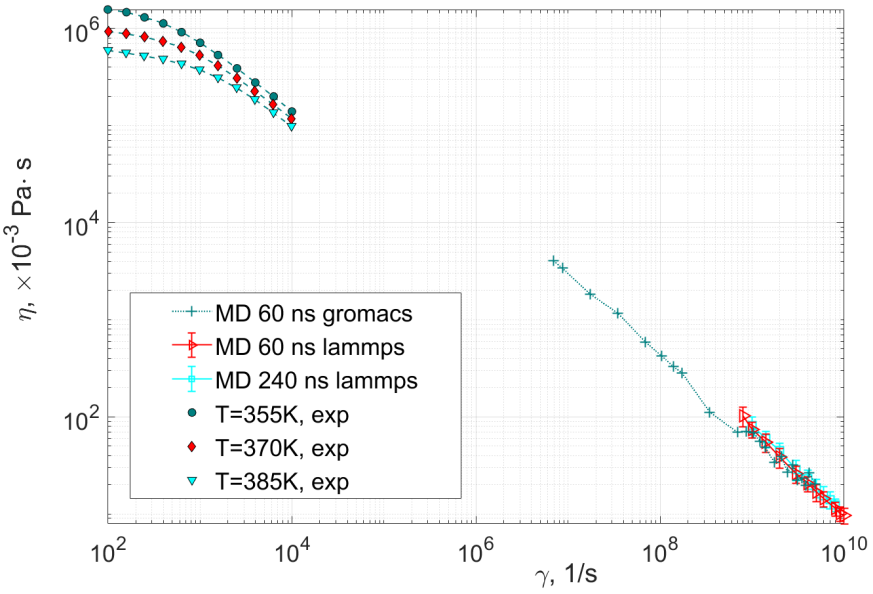

Figure 9: Comparison between experimental results (upper left corner) and MD simulations (lower right corner). The experimental results were obtained[66] for Ultem 1000 at three different temperatures: 355 ℃ (teal circles), 370 ℃ (red diamonds), and 385 ℃ (cyan triangles). The MD results were obtained at T = 325 ℃ using LAMMPS (the same as in Fig. 8) for 60 ns (red open triangles) and 240 ns (cyan open squares) and using GROMACS for 240 ns (green plusses). (color online)

The shear-thinning behavior and weak dependence of $\eta(T)$ on surface viscosity obtained in MD simulations suggest that the observed values of η are close to bulk values. It is therefore interesting to compare the dependence of $\eta(\gamma)$ obtained in MD estimations with experimental data.

To facilitate comparison of the estimated η values with experimental data, we have extended MD simulations to deformation rates of $\sim 6.9 \times 10^6$ 1/s using GROMACS on Amazon Web Services. The results of the extended simulations are compared with experimental data[66] in Fig. 9. We note that the MD predictions are in even better agreement with the experimental data obtained for Ultem 9085 at room temperature[71].

These results demonstrate that atomistic simulations are capable of quantitative estimation of the shear viscosity in PEI/PC blends but are weakly sensitive to changes in the interface values of η.

CONCLUSIONS

We have developed an atomistic model of polyetherimide/polycarbonate blends with planar polymer-polymer interfaces. It takes explicit account of electrostatic interactions and the semi-flexible nature of the chains. We used molecular dynamics simulations of this model to analyze diffusion and strengthening as a function of welding time during the first 300 ns.

It was shown that welding occurs in a number of steps. The initial gap at the interface between the two pieces of polymer was closed on a time scale of a few pico-seconds in the well-known "wetting" process[1,63].

During the second step we observed fast interfacial diffusion, attributable to the initial existence of un-equilibrated chain ends and "vacancies" on the both sides of the interface. This fast diffusion occurred on a timescale of 20-30 ps. During this process the diffusion of chain ends at the interface occurs via the two distinct mechanisms of reptation[1,5,6] and Eyring-type[64] jumps between quasi-equilibrium positions of chain ends.

Finally, we observed slow interfacial diffusion, dominated by reptation, and corresponding to the equilibration of center-of-mass (CM) distributions of polymer chains. It was shown that equilibration has two timescales corresponding to the two components of the blend. In particular, the CM distribution of PC chains approaches quasi-equilibrium on a time scale of the order of 100 ns, while the CM distribution of the PEI chains remains nonuniform up to 300 ns.

Strengthening of the channels as a function of welding time was analyzed by simulating uni-axial elongation of quenched (to 300 K) samples after 60 and 240 ns of equilibration and after additional thermal cycling of the samples between 300 and 600 K. It was shown that Young's modulus E is increased when the welding time is changed from 60 ns to 240 ns. Changes of E are much less pronounced for further increase of welding time during thermal cycling while the yield strength of the samples continues to increase.

The observed features were attributed to the slow CM diffusion of PEI and PC chains. The increase of yield strength during thermal cycling corresponds to the slow equilibration of the CM distribution of PEI chains in accordance with Wool's criterion[6].

We note that the breakup in all samples, except the breakages obtained after thermal

cycling, was due to the pulling out of chains at the interface, which remained the weakest part of the system. After thermal cycling, breakup could occur at different locations indicating that almost the full strength of the interface had been recovered.

The shear viscosity η was estimated using MD simulations of uni-diagonal deformation of the samples quenched to 300 K after 60 and 240 ns of welding. It was shown that both samples exhibited the shear-thinning behavior characteristic of polymer melts[69]. The dependence of η on the shear rate was shown to be in good agreement with available experimental data. However, we observed only weak (within the error of estimation) dependence of η on welding time in the simulations.

The thermal, mechanical, and optical properties obtained for welded samples also exhibit good agreement with available experimental data as will be discussed in detail in a separate paper[39].

In conclusion, the results obtained demonstrate that fully atomistic models can be used to make realistic estimates of the parameters of welded polymer interfaces, and to anchor continuous models of polymer-based manufacturing processes. In particular, using obtained results we conjecture that the strengths of interfaces in polyetherimide blends (and parts produced using additive manufacturing) may be improved by reducing the molecular weight of PEI chains and by broadening their molar mass distribution. However, further more detailed research will be needed to verify this conjecture. The revealed features of the polymer dynamics at the interface are characteristic for semiflexible chains with partial charges and the results obtained could be useful for further development of the theory for such polymers.

It is also expected that the modeling approach developed in this work will help to elucidate specific features of materials and enhance physics-based characterization of polymer parts manufactured in space under micro-gravity conditions.

The main limitation of our results relates to the relatively small sizes of the samples and polymer chains. Fully atomistic simulation of the interface welding in larger models will be performed in future work.

ACKNOWLEDGMENTS

We thank Gabriel Jost for the help in running simulations on Amazon Web Services. We acknowledge financial support by the Leverhulme Trust Research Project Grant RPG-2017-134, by the NASA STMD/GCD/LSM grant in Space Manufacturing, and by the Engineering and Physical Science Research Council under Grant No. EP/M015831/1.

References

1. S. Prager and M. Tirrell, J. Chem. Phys. **75**, 5194 (1981).
2. I. C. Sanchez, ed., *Physics of Polymer Surfaces and Interfaces* (Elsevier Science, 2013).
3. T. Ge, M. O. Robbins, D. Perahia, and G. S. Grest, Phys. Rev. E **90**, 012602 (2014).
4. Y. H. Kim and R. P. Wool, Macromolecules **16**, 1115 (1983).
5. M. Doi and S. F. Edwards, *The Theory of Polymer Dynamics*, International series of monographs on physics (Clarendon Press, 1988).
6. R. P. Wool, *Polymer Interfaces: Structure and Strength* (Hanser Publishers, 1995).
7. R. A. L. Jones, R. W. Richards, and M. Muthukumar, Phys. Today **53**, 59 (2000).
8. A. E. Likhtman and R. S. Graham, J. Non-Newtonian Fluid Mech. **114**, 1 (2003).
9. Q. Sun, G. M. Rizvi, C. T. Bellehumeur, and P. Gu, Rapid Prototyping Journal **14**, 72 (2008).
10. C. McIlroy and P. D. Olmsted, J. Rheol. **61**, 379 (2017).
11. J. Bartolai, T. W. Simpson, and R. Xie, Rapid Prototyping Journal pp. 00–00 (2018).
12. A. Owens and O. D. Weck, in *AIAA SPACE 2016* (American Institute of Aeronautics and Astronautics, 2016).
13. X.-Y. Wang, P. J. i. in't Veld, Y. Lu, B. D. Freeman, and I. C. Sanchez, Polymer **46**, 9155 (2005).
14. J. Xia, S. Liu, P. K. Pallathadka, M. L. Chng, and T.-S. Chung, Ind. Eng. Chem. Res. **49**, 12014 (2010).
15. S. G. Falkovich, S. V. Lyulin, V. M. Nazarychev, S. V. Larin, A. A. Gurtovenko, N. V. Lukasheva, and A. V. Lyulin, J. Polym. Sci. B Polym. Phys. **52**, 640 (2014).

16. S. G. Fal'kovich, S. V. Larin, V. M. Nazarychev, I. V. Volgin, A. A. Gurtovenko, A. V. Lyulin, and S. V. Lyulin, Polym. Sci. Series A **56**, 558 (2014).

17. V. M. Nazarychev, A. Y. Dobrovskiy, S. V. Larin, A. V. Lyulin, and S. V. Lyulin, J. Polym. Sci. B Polym. Phys. **56**, 375 (2017).

18. A. Bagsik, V. Schöppner, and E. Klemp, Proceedings of International Conference Polymeric Materials pp. 1–8 (2010).

19. A. Gebhardt, *Additive Manufacturing: 3D Printing for Prototyping and Manufacturing* (Hanser, 2016).

20. R. J. Zaldivar, D. B. Witkin, T. McLouth, D. N. Patel, K. Schmitt, and J. P. Nokes, Additive Manufacturing **13**, 71 (2017).

21. K. P. Motaparti, G. Taylor, M. C. Leu, K. Chandrashekhara, J. Castle, and M. Matlack, Virtual Phys. Prototyp. **12**, 207 (2017).

22. I. Gajdos and J. Slota, Technical Gazette **20**, 231 (2013).

23. F. Pierce, D. Perahia, and G. S. Grest, EPL **95**, 46001 (2011).

24. T. Ge, F. Pierce, D. Perahia, G. S. Grest, and M. O. Robbins, Phys. Rev. Lett. **110** (2013).

25. C. Li and A. Strachan, Polymer **52**, 2920 (2011).

26. B. E. Eichinger, D. Rigby, and J. Stein, Polymer **43**, 599 (2002).

27. M. Zhang, P. Choi, and U. Sundararaj, Polymer **44**, 1979 (2003).

28. S. V. Lyulin, A. A. Gurtovenko, S. V. Larin, V. M. Nazarychev, and A. V. Lyulin, Macromolecules **46**, 6357 (2013).

29. A. de Nicola, A. Correa, G. Milano, P. L. Manna, P. Musto, G. Mensitieri, and G. Scherillo, J. Phys. Chem. B **121**, 3162 (2017).

30. K. Yokomizo, Y. Banno, and M. Kotaki, Polymer **53**, 4280 (2012).

31. M. Bulacu and E. van der Giessen, J. Chem. Phys. **123**, 114901 (2005).

32. J. Baschnagel, H. Meyer, J. Wittmer, I. Kulić, H. Mohrbach, F. Ziebert, G.-M. Nam, N.-K. Lee, and A. Johner, Polymers **8**, 286 (2016).

33. H.-P. Hsu and K. Kremer, J. Chem. Phys. **144**, 154907 (2016).

34. R. Faller, Macromolecules **37**, 1095 (2004).

35. I. M. de Arenaza, E. Meaurio, and J.-R. Sarasu, in *Polymerization* (InTech, 2012).

36. H. Wang, B. Shentu, and R. Faller, Phys. Chem. Chem. Phys. **17**, 4714 (2015).

37. P. Bajaj, D. Bajaj, C. Strom, H. Zhou, and K. Leung, Microsc. Microanal. **21**, 613 (2015).

38. G. Cicala, G. Ognibene, S. Portuesi, I. Blanco, M. Rapisarda, E. Pergolizzi, and G. Recca, Materials **11**, 285 (2018).

39. D. G. Luchinsky, H. Hafiychuk, V. Hafiychuk, K. Chaki, H. Yoshida, T. Ozawa, K. R. Wheeler, T. J. Prater, and P. V. E. McClintock, to be submitted (2020).

40. T. G. Fox and S. Loshaek, Journal of Polymer Science **15**, 371 (1955).

41. *User's Manual, J-OCTA Overview, J-OCTA 4.0*, JSOL corp. (2018).

42. S. Plimpton, Tech. Rep. AND91–1144, Sandia National Laboratories (1993).

43. T. W. Sirk, S. Moore, and E. F. Brown, J. Chem. Phys. **138**, 064505 (2013).

44. H. J. C. Berendsen, D. van der Spoel, and R. van Drunen, Comput. Phys. Commun. **91**, 43 (1995).

45. E. Lindahl, B. Hess, and D. van der Spoel, J. Mol. Model. **7**, 306 (2001).

46. S. Páll, M. J. Abraham, C. Kutzner, B. Hess, and E. Lindahl, in *Lecture Notes in Computer Science* (Springer International Publishing, 2015), pp. 3–27.

47. *NASA Advanced Supercomputing Division*, https://www.nas.nasa.gov/index.html (2019).

48. *Amazon web services, inc*, https://aws.amazon.com/?nc2=h_lg (2019).

49. M. P. Allen, *Computer Simulation of Liquids* (OUP Oxford, 2017).

50. S. L. Mayo, B. D. Olafson, and W. A. Goddard, J. Phys. Chem. **94**, 8897 (1990).

51. J. J. P. Stewart, J. Mol. Model. **19**, 1 (2012).

52. T. Darden, L. Perera, L. Li, and L. Pedersen, Structure **7**, R55 (1999).

53. R. W. Hockney and J. W. Eastwood, *Computer Simulation Using Particles* (CRC Press, 1988).

54. R. Pan, W. Zhao, T. Zhou, and A. Zhang, Journal of Polymer Science Part B: Polymer Physics **48**, 595 (2010).

55. H. Sun, The Journal of Physical Chemistry B **102**, 7338 (1998).

56. C. Li, G. A. Medvedev, E.-W. Lee, J. Kim, J. M. Caruthers, and A. Strachan, Polymer **53**, 4222 (2012).

57. D. G. Luchinsky, H. Hafiychuk, V. Hafiychuk, and K. R. Wheeler, Tech. Rep. NASA/TM-2018-220213, NASA Ames Research Center (2018).

58. S. V. Lyulin, S. V. Larin, A. A. Gurtovenko, V. M. Nazarychev, S. G. Falkovich, V. E. Yudin, V. M. Svetlichnyi, I. V. Gofman, and A. V. Lyulin, Soft Matter **10**, 1224 (2014).

59. V. M. Nazarychev, A. V. Lyulin, S. V. Larin, A. A. Gurtovenko, J. M. Kenny, and S. V. Lyulin, Soft Matter **12**, 3972 (2016).

60. L. D. Landau, E. M. Lifshitz, A. M. Kosevich, J. B. Sykes, L. P. Pitaevskii, and W. H. Reid, *Theory of Elasticity*, Course of theoretical physics (Elsevier Science, 1986).

61. S. J. L. Kang, *Sintering: Densification, Grain Growth and Microstructure* (Elsevier Science, 2004).

62. T. Aoyagi, Nihon Reoroji Gakkaishi **37**, 75 (2009).

63. E. Jabbari and N. A. Peppas, Journal of Macromolecular Science, Part C: Polymer Reviews **34**, 205 (1994).

64. R. H. Ewell and H. Eyring, J. Chem. Phys. **5**, 726 (1937).

65. S. Plimpton, J. Comput. Phys. **117**, 1 (1995).

66. *ULTEM 9085, stratasys ltd* (2019).

67. *ULProspector.com from UL, LLC*, https://www.protolabs.com/media/1014801/ultem-1000-im.pdf (2018).

68. Q. Zheng and J. C. Mauro, J. Am. Ceram. Soc. **100**, 6 (2016).

69. T. A. Osswald and N. Rudolph, *Polymer Rheology: Fundamentals and Applications* (Hanser Publications, 2015).

70. M. Joly, J. Colloid Sci. **11**, 519 (1956).

71. Y. Seo, J. Kim, and H.-J. Kim, Polymer Engineering & Science **42**, 2401 (2002).